POLITECNICO DI TORINO
Repository ISTITUZIONALE

Game-theoretic modeling of collective decision making during epidemics

(Article begins on next page)

08 November 2022

Game-theoretic modeling of collective decision-making during epidemics

Mengbin Ye[1], Lorenzo Zino[2], Alessandro Rizzo[3],* and Ming Cao[2]

[1] *Optus–Curtin Centre of Excellence in Artificial Intelligence, Curtin University, Perth, Australia*
[2] *Faculty of Science and Engineering, University of Groningen, 9747 AG Groningen, Netherlands*
[3] *Dipartimento di Elettronica e Telecomunicazioni, Politecnico di Torino, 10129 Torino, Italy*
(Dated: July 19, 2021)

The spreading dynamics of an epidemic and the collective behavioral pattern of the population over which it spreads are deeply intertwined and the latter can critically shape the outcome of the former. Motivated by this, we design a parsimonious game-theoretic behavioral–epidemic model, in which an interplay of realistic factors shapes the co-evolution of individual decision-making and epidemics on a network. Although such a co-evolution is deeply intertwined in the real-world, existing models schematize population behavior as instantaneously reactive, thus being unable to capture human behavior in the long term. Our model offers a unified framework to model and predict complex emergent phenomena, including successful collective responses, periodic oscillations, and resurgent epidemic outbreaks. The framework also allows to assess the effectiveness of different policy interventions on ensuring a collective response that successfully eradicates the outbreak. Two case studies, inspired by real-world diseases, are presented to illustrate the potentialities of the proposed model.

INTRODUCTION

The collective adoption of appropriate behavior by a population is crucial to respond to an epidemic, especially when pharmaceutical interventions are absent or logistical challenges prevent their widespread deployment [1, 2]. However, classical mathematical epidemic models often consider oversimplified behavioral response [3]. To fill in this gap, awareness-based models have been proposed [4–12], in which the epidemic process co-evolves with the spread of the awareness of the outbreak. While these models have demonstrated effectiveness in capturing the early-stage, immediate behavioral response to an epidemic, they are limited because they assume fully rational, purely instantaneous, and reactive decision-making in the population. Such models therefore fail to capture the very range of factors that affect real-world behavioral responses over the whole course of an epidemic, such as social influence [13], perceived infection risk [14], accumulating fatigue and socio-economic costs [15, 16], bounded rationality in individuals' decisions [17], and the impact of government-mandated interventions [18, 19].

The world is not new to epidemics that evolve over long time horizons of several months or even years, persisting until effective drugs and vaccines are developed and then made widely available [20], making purely reactive models of limited efficacy. This calls for a paradigm shift in mathematical modeling, from reactive and fully rational behavioral responses [4–7, 9, 10], to a long-term outlook where complex behavioral dynamics arise at the individual-level and co-evolve at the same time scale of the epidemic spreading. Game-theoretic models have proved to be effective to reproduce similar complex decision-making mechanisms, thereby capturing realistic behavioral responses in several fields [21].

Here, we propose a game-theoretic model that is specifically designed to account for long-term and bounded-rational decision-making, and show it is able to reproduce the complex and concurrent evolution of behavioral response and epidemic spreading that is well-known and documented in the real-world [1]. Several efforts have been proposed across similar research avenues, although with different and narrower angles. For example, imitation mechanisms [14, 16, 22, 23] rely on a population-level modeling that can capture only limited features of such complex behavioral dynamics. Recently, an individual-level imitation-driven mechanism that accounts for the perceived risk of infection and immediate costs for adopting protective behaviors has been proposed and analyzed, showing that it may generate sustained steady oscillations [24, 25]. Following a different approach, game-theoretic modeling of vaccination adoption have been proposed [26–32]. These models rely on a time-scale separation between the epidemic spreading and the behavioral decision, which is typically made just at the beginning of each epidemic season. However, such a time-scale separation does not capture general behavioral response.

Here, we adopt a network approach with individual granularity [3] and a co-evolution of the two processes, at the same time scale, under the impact of the entire range of factors discussed in the above (i.e., including perceived risk, immediate costs, accumulating fatigue, social influence, and bounded rationality). Hence, our model is designed to be able to capture the individual-level responses and time-varying contagion patterns, whose *co-evolution* collectively shapes the epidemic outbreak. Our approach enables the *explicit and concurrent* inclusion of the most salient factors that each individual trades off when deciding their time-varying behavioral response to an ongoing epidemic. The central contribution of our work is the design of a unified and parsimonious mathematical framework for the co-evolution of the decision-making and the epidemic outbreak, which can be coupled with any existing compartmental model [33], and thus it can be tailored to study the key features of any real-world disease. As we shall illustrate through some simple case studies, the proposed framework is able to capture and reproduce complex realistic behavioral response by the population, including successful collective responses leading to the eradication of the

---

* Also at Office of Innovation, New York University Tandon School of Engineering, 11201 Brooklyn NY, USA
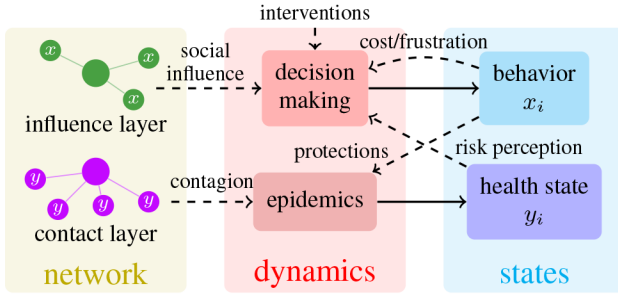
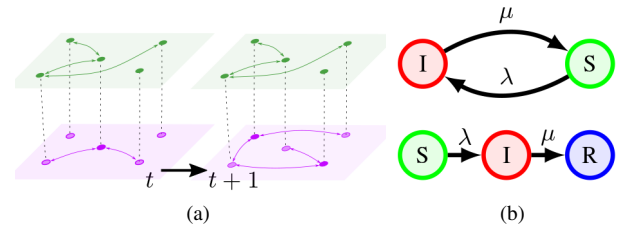FIG. 1: Schematic of the co-evolutionary paradigm.

FIG. 2: Illustration of the network model and the epidemic progression. In (a), two time-steps in the two-layer network representation. The upper layer (green) shows the static influences, the lower layer (violet) time-varying physical contacts. In (b), state transitions of the SIS (above) and SIR models (below).

disease, periodic oscillations, and weak responses leading to the emergence of multiple epidemic waves.

MODEL

We consider a population $\mathcal{V}$ of n individuals. Each individual $i \in \mathcal{V}$ is characterized by a two-dimensional variable $(x_i(t), y_i(t))$, which models their *social behavior* and *health state* at the discrete time $t \in \mathbb{Z}_{\geq 0}$, respectively. The social behavior of individual i is captured by the binary variable $x_i(t) \in \{0, 1\}$, which expresses whether i adopts self-protective behaviors ($x_i(t) = 1$), such as physical distancing [1], or discards this opportunity ($x_i(t) = 0$). The health state $y_i(t)$ takes values in a discrete set of compartments $\mathcal{A}$. For example, $\mathcal{A} = \{S, I\}$ is selected to model the susceptible–infected–susceptible (SIS) epidemic process exemplified in this work [33]. A global observable $z(t)$ quantifies the *detectable prevalence* of the epidemic at time t: $z(t) := \frac{1}{n} |\{i : y_i(t) = I\}|$, where $|\cdot|$ denotes a set's cardinality. The paradigm is amenable to extensions to capture different levels of protection through the selection of a different support for $x_i(t)$, while further compartments added to $\mathcal{A}$ can capture additional features of the epidemic process [33].

The decision-making and disease spreading in the population co-evolve, mutually influencing each other on a two-layered network $\mathcal{G} = (\mathcal{V}, \mathcal{E}_I, \mathcal{E}_C(t))$ [34], as schematized in Fig. 1. The set of undirected links $\mathcal{E}_I$ defines the static *influence layer*, capturing *social influence* between individuals in their decision-making processes. The *contact layer* is defined through a time-varying set of undirected links $\mathcal{E}_C(t)$, which represent the *physical contacts* between pairs of individuals that are the avenues for the transmission of the disease. The temporal formation mechanism of the contact layer, illustrated in Fig. 2a, is general and can be generated according to any model of time-varying networks [35–40].

At each discrete time-step t, every individual i enacts a decision-making process on the adoption of self-protective behaviors, according to an evolutionary game-based mechanism termed logit learning [41]. We define two *payoff* functions $\pi_i^0(t)$ and $\pi_i^1(t)$, which represent a combination of socio-psychological, economic, and personal benefits received by individual i for enacting behaviors $x_i = 0$ and $x_i = 1$ at time t, respectively. This individual then adopts self-protective be-

haviors with a probability equal to

$$\mathbb{P}[x_i(t+1) = 1] = \frac{\exp\{\beta \pi_i^1(t)\}}{\exp\{\beta \pi_i^0(t)\} + \exp\{\beta \pi_i^1(t)\}}; \quad (1)$$

otherwise the individual will adopt $x_i(t+1) = 0$. The parameter $\beta \in [0, \infty)$ measures an individual's *rationality* in the decision-making process. We have assumed for simplicity that β is homogeneous among all individuals, but this is easily generalizable to a heterogeneous β_i distribution. Notice that if $\beta = 0$, individuals make decisions uniformly at random, while for $\beta \to \infty$, individuals apply perfect rationality to select the behavior with highest payoff. This best-response behavior is myopic, i.e., individuals do not look forward in time to optimize a sequence of decisions. Myopic behavior is reasonable given the uncertain nature of a long-lasting epidemic.

Payoffs are defined as

$$\pi_i^0(t) := \frac{1}{d_i} \sum_{j:(i,j) \in \mathcal{E}_I} \left(1 - x_j(t)\right) - u(t), \quad (2a)$$

$$\pi_i^1(t) := \frac{1}{d_i} \sum_{j:(i,j) \in \mathcal{E}_I} x_j(t) + r\big(z(t)\big) - f_i(t), \quad (2b)$$

where $d_i := |\{j : (i,j) \in \mathcal{E}_I\}|$ is the degree of node i on the influence layer, and contain the following four terms, directly related to behavioral and social factors that shape the epidemic dynamics.

Social influence. The first term in Eqs. (2a)–(2b), inspired by network coordination games [42], captures the *social influence* of neighboring individuals and the individual's desire to coordinate with them on the behavioral response [13]. The role of social influence should be understood by viewing the first terms of Eq. (2a) and Eq. (2b) together; as more of the neighbors of individual $i \in \mathcal{V}$ adopt self-protection or do not adopt self-protection, then individual i also has more incentive to adopt or not adopt, respectively. This ensures that individuals tend to conform and coordinate with one another; coordination and conformity are prevalent factors for many different human behaviors, including social norms and conventions [43–45], diffusion of social innovation [46, 47], and

also in individuals' decisions concerning the *behavioral response* to epidemics [13].

Policy interventions. The time-varying term $u(t) \geq 0$ in Eq. (2a) represents the impact of *nonpharmaceutical interventions* enforced by public authorities to discourage dangerous behaviors, e.g., lockdowns, see [19] for more details.

Risk perception. The *risk-perception function* $r(z) : [0,1] \rightarrow \mathbb{R}_{\geq 0}$ in Eq. (2b) is a monotonically nondecreasing function of the detectable prevalence z, which models the population's reaction to the spread of the disease. This function is amenable to several generalizations, e.g., to capture imperfect or delayed information due to real-world testing logistics, or heterogeneity of the function in the population. In its simplest formulation (which is adopted in the case studies presented in this paper), it can be assumed to be a power function $r(z) = kz^{\alpha}$, with $k > 0$ as a scaling factor and $\alpha > 0$ that determines the characteristics of the population. Specifically, $\alpha \in (0,1)$ models cautious populations, where a small initial outbreak causes a large increase in the risk perception; $\alpha = 1$ captures a population whose reaction grows linearly with the epidemic prevalence observed; and $\alpha > 1$ captures populations that underestimate the risk, and the epidemic prevalence must be large before the risk perception plays an important role in the decision-making process.

Cost of self-protective behavior. The negative impact of adopting self-protections is captured in Eq. (2b) by the *frustration function*

$$f_i(t) = c + \sum_{s=1}^{t} \gamma^s c x_i(t-s), \tag{3}$$

where $c \geq 0$ quantifies the social, psychological, and economic *immediate cost* per unit-time, e.g., related to the inability to socialize, work from the office, enjoy public spaces, etc., and $\gamma \in [0,1]$ is the *accumulation factor* [16, 48]. When $\gamma = 0$, an individual accounts only for the immediate cost, and as γ increases, the impact of all past decisions on the payoff increases. This may reflect the accumulating nature of fatigue, stress, and economic losses [15, 16, 48]. Thus, $f_i(t) \geq 0$ reflects accumulative costs for individual i up to time t. Note that the function $f_i(t)$ could be extended by adding further features of the frustration mechanism, including nonlinearities.

To summarize, the payoff that an individual $i \in \mathcal{V}$ would receive for not adopting self-protective behavior in Eq. (2a) is equal to the difference of two terms. Besides the social influence term, the other term reduces the payoff to represent the implementation of policies to disincentivize nonprotective behaviors; the effectiveness of policies in shaping behaviors has been extensively analyzed in the recent literature [18, 19]. The payoff for adopting self-protective behavior in Eq. (2b), instead, is equal to the sum of two positive contributions, and decreased by a third one. The first term accounts for the social influence. The second term, associated with the risk perception, captures an increased incentive to adopt self-protective behavior due to the endogenous fear of increased risk to infection as the disease spreads (and conversely, a lower risk is

TABLE I: Notation.

n	population size	λ	infection probability
$\mathcal{E}_I$	influence layer edges	μ	recovery probability
$\mathcal{E}_C(t)$	contact layer edges	β	rationality
$N_i(t)$	infectious contacts of i	$u(t)$	policy interventions
σ	efficacy of self-protections	$r(z)$	risk perception function
$x_i(t)$	behavior of i	c	immediate cost
$y_i(t)$	health state of i	γ	accumulation factor
$z(t)$	detected prevalence	$f_i(t)$	frustration function of i

perceived as the epidemic dwindles due to the growing optimism of returning to normal). This term has some analogies to the mechanism of purely reactive awareness-based models, but which do not consider the other factors detailed above [4–12]. A similar implementation of this term is often present in the payoffs of imitation-based game-theoretic models [14, 16, 22, 23, 25]. Finally, the last term reduces the payoff to account for the immediate and accumulated social, psychological, and economic costs associated with the adoption of self-protective behavior [15, 48]. A similar term — without the accumulation mechanism— has been considered in some imitation-based models [25].

Concurrently with the behavioral decision, at each timestep t, every individual i that does not adopt self-protections and is susceptible (i.e., $x_i(t) = 0$ and $y_i(t) = S$) may become infected upon contact with an infected individual $j : y_j(t) = I$, with a per-contact *infection probability* $\lambda \in [0,1]$. We introduce a parameter $\sigma \in [0,1]$ that represents the *effectiveness* of self-protective behavior in preventing contagion, and we assume that the adoption of self-protection, $x_i(t) = 1$, does not affect the individual's probability of transmitting the disease. Hence, considering an SIS epidemic model (see Fig. 2b), the contagion probability for individual $i \in \mathcal{V}$ evolves in time as

$$\mathbb{P}[y_i(t+1) = I | y_i(t) = S] = \\ = (1 - \sigma x_i(t))\Big(1 - (1-\lambda)^{N_i(t)}\Big), \tag{4}$$

where

$$N_i(t) := |\{j \in \mathcal{V} : (i,j) \in \mathcal{E}_C(t), y_j(t) = I\}| \tag{5}$$

is the number of infectious physical contacts of node i at time t. Note that the model can be extended to account for mutual protection by adding an additional parameter and expanding the term $N_i(t)$, depending on the behavior of the neighbors. Besides the contagion, at each time-step t, every infected individual i recovers with probability $\mu \in (0,1]$, becoming susceptible again to the disease, i.e.,

$$\mathbb{P}[y_i(t+1) = S | y_i(t) = I] = \mu. \tag{6}$$

Table I summarizes the notation.

RESULTS

In the following, we opt for modeling the contact layer $\mathcal{E}_C(t)$ by means of a discrete-time activity-driven network
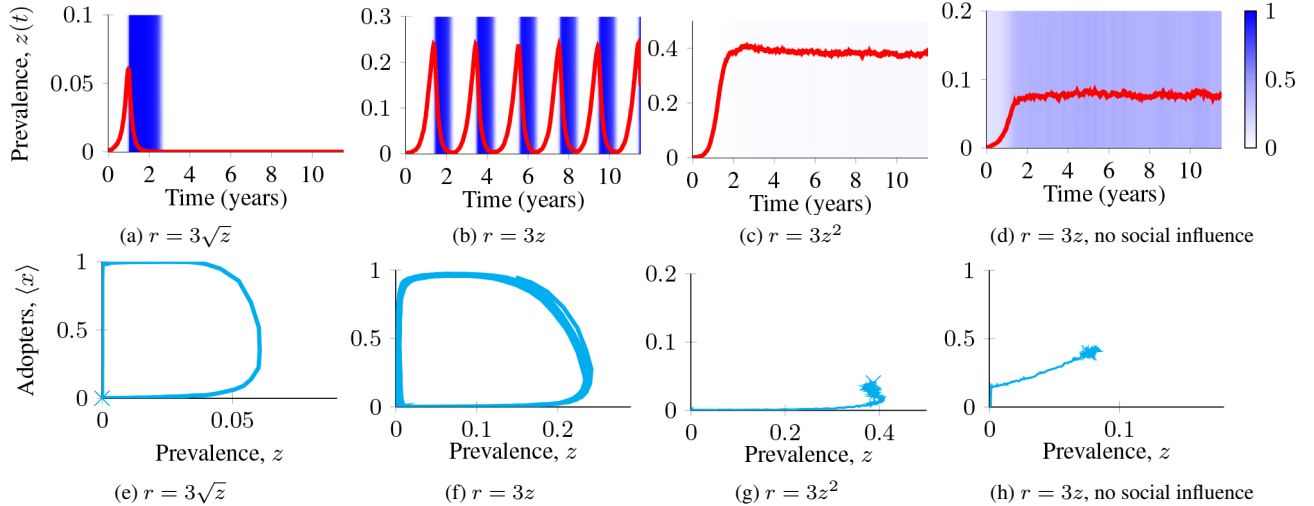
FIG. 3: Simulations of the SIS model. In (a)–(d), we show the time-evolution of the epidemic prevalence $z(t)$ (red) and the fraction of adopters of self-protections $\langle x(t) \rangle := \frac{1}{n} \sum_{i \in \mathcal{V}} x_i(t)$ (intensity of the blue bands). In (e)–(h), we show the corresponding trajectories on the phase-space. Panels refer to different risk perceptions $r(z)$, as detailed in the sub-captions.

(ADN) [36], which has found successful application in mathematical epidemiology [49]. In ADNs, each individual $i \in \mathcal{V}$ is characterized by a constant parameter $a_i \in [0,1]$, called *activity*, which quantifies their probability to be "active" and thus generate a fixed number $m \geq 1$ of undirected links with other individuals selected uniformly at random from the population, for each discrete-time step t. Similar to its original formulation, we choose m to be constant and equal for all individuals. These contacts are added to the link set $\mathcal{E}_C(t)$, contribute to the epidemic process, and are then removed before the next discrete time instant and the next activation of individuals. Despite their simplicity, which enables rigorous analytical treatment and fast numerical simulations [36, 39], ADNs can capture important features of complexity that characterize real-world networks, including their temporal and heterogeneous nature, and further features can be incorporated in an analytically-tractable manner [50–53].

Epidemic threshold

For large populations and fully connected influence layers, we compute the epidemic threshold via a mean-field approach [54]. In the absence of cumulative frustration ($\gamma = 0$), which is a reasonable assumption in the early stages of an outbreak, and assuming constant policy interventions $u(t) = \bar{u}$, the outbreak is quickly eradicated if

$$\frac{\lambda}{\mu} < \frac{e^{\beta(1-\bar{u})} + (1-\beta)e^{-\beta c}}{m(\langle a \rangle + \sqrt{\langle a^2 \rangle})(e^{\beta(1-\bar{u})} + (1-\beta-\sigma)e^{-\beta c})}, \quad (7)$$

where $\langle a \rangle := \frac{1}{n} \sum_{i \in \mathcal{V}} a_i$ and $\langle a^2 \rangle := \frac{1}{n} \sum_{i \in \mathcal{V}} a_i^2$ are the mean and second moment of the activity distribution, respectively (the derivation of Eq. (7) is reported in Appendix A). Note that, when the cost for adopting self-protections grows

large, $c \to \infty$, the threshold in Eq. (7) tends to the same threshold expression as that of a standard SIS model on ADNs, which is $\lambda/\mu < (m(\langle a \rangle + \sqrt{\langle a^2 \rangle}))^{-1}$ [36].

The threshold in Eq. (7) offers insight into the role of human behavior in the early stages of an epidemic outbreak by establishing conditions under which the disease is immediately eradicated. However, the key novelty of the proposed paradigm lies in the possibility to investigate the interplay between human behavior and epidemic spreading in the long term, when the epidemic actually spreads (i.e., above the epidemic threshold). In this scenario, such a complex interplay may give rise to several interesting and realistic phenomena, such as periodic oscillations and multiple waves, the emergence of endemic diseases, and even behavioral responses leading to the successful eradication of the outbreak. In the following, we execute a numerical study to elucidate such phenomena [55]. Specifically, we combine our co-evolutionary model with the classical SIS and susceptible–infected–recovered (SIR) models, parametrized to reproduce real-world diseases. The SIS model is used to illustrate the large variety of phenomena that the paradigm can reproduce, and to discuss the key role of social influence into determining a collective response, confirming recent empirical evidence from the social psychology literature [13]. The SIR model is utilized to show that our model can reproduce real-world epidemic patterns, and to discuss the design of policy interventions. In all the simulations, we fix $n = 20,000$ individuals (20 of them initially infected, selected uniformly at random). The influence layer is modeled through a Watts–Strogatz small-world network [56] with average degree 8 and rewiring probability $1/8$. The contact layer is generated through an ADN with power-law distributed activities a_i with a negative exponent -2.09, as in [57], and lower cutoff at $a_{\min} = 0.1$.

SIS model

We simulate an SIS model calibrated on gonorrhea [58] (see Appendix B and Table II), by fixing an immediate cost of $c = 0.3$ with no accumulation $\gamma = 0$ and assuming that no policy interventions are enacted ($u(t) = 0$, $\forall t \geq 0$). In Figs. 3a–3c, we consider three scenarios with progressively less cautious populations ($r(z) = 3\sqrt{z}$, $r(z) = 3z$, and $r(z) = 3z^2$, respectively, see Appendix B). We observe that this shift in risk perception causes not only a quantitative shift in the epidemic dynamics, similar to most awareness-based models [6, 7], but more importantly, qualitatively changes the salient phenomena. In fact, the phenomena spans from a prompt and sustained collective response that leads to fast eradication of the disease (in Fig. 3e, the trajectory rapidly reaches the disease-free manifold $z = 0$), to periodic oscillations both in the epidemic prevalence and in the behavioral response (Figs. 3b and 3f), and finally to a partial behavioral response, resulting in the emergence of a meta-stable endemic equilibrium (Figs. 3c and 3g). The periodic oscillations are similar to that observed in several existing works, such as [24, 25].

In the scenario depicted above, the risk perception function determines a critical prevalence $z^* = \min\{z : r(z) > 1 + c\}$, such that $z(t) > z^*$ implies that the payoff for adopting self-protections is larger than for not adopting them ($\pi_i^1(t) > \pi_i^0(t)$), for any individual, irrespective of the behavior of others. With $r(z) = 3\sqrt{z}$, the critical prevalence is $z^* \approx 18\%$. However, as can be observed in Fig. 3e, social influence causes individuals to rapidly and widely adopt self-protective behaviors at a much earlier prevalence of $z \approx 6\%$, highlighting the key role played by social influence toward facilitating the emergence of collective behavioral patterns and, in this instance, helping in the fast eradication of the disease.

We further investigate the role of social influence by simulating the model in its absence (i.e., removing the first term in Eqs. (2a)–(2b), as detailed in Appendix C). Our findings support the intuition that social influence is key to ensure collective population responses, which are in turn crucial for the successful eradication of the disease (Fig. 3a) and the emergence of periodic oscillations (Fig. 3b). In fact, in the absence of social influence, the system shows a less rich range of behaviors, whereby a partial behavioral response always leads to the convergence to an endemic equilibrium (Figs. 3d and 3h are obtained with the parameters of Fig. 3b without social influence. However, interestingly, social influence can also cause collective rejection of self-protective behaviors, and this results in a higher peak disease prevalence with respect to the scenario without social influence. Simulations corresponding to Figs. 3a and 3c are reported in Appendix C (Fig. 5).

SIR model

We further elucidate the potentialities of our behavioral paradigm by combining it with an SIR model (see Fig. 2a). In the SIR model, the *removed* (R) health state is added to $\mathcal{A}$ to represent immunized individuals after recovery (or death),

and the system is governed by Eq. (4) and $\mathbb{P}[y_i(t + 1) = R \,|\, y_i(t) = I] = \mu$. The model is calibrated on the 1918–19 Spanish flu [59, 61] (see Appendix B and Table II). In particular, we set a risk perception function that increases slowly, $r = 3z^2$ (associated with the initial suppression of news about the flu [62]), and policy interventions are set to mimic historical lockdowns ($u(t) = 0.5$ when 1% of the population is infected, and held constant for $T_a = 28$ days [60]). For airborne diseases like Spanish flu, self-protective behaviors entail physical distancing and closures of economic activities, which often yield an accumulation of psychological distress and economic losses [15, 48, 63]. Accordingly, we set $c = 0.1$ and $\gamma = 0.9$ (see Appendix B). Figure 4a shows that our paradigm is able to qualitatively reproduce the historical epidemic pattern, which witnessed a resurgent pandemic with three waves that includes a massive second wave [59, 60].

We utilize this example to discuss the design of policy interventions. First, from Fig. 4b, we observe that mild policy interventions, even if indefinite in duration ($u(t) = 0.4$, $\forall t \geq 0$), may not be sufficient to ensure a timely and collective response, resulting in a massive outbreak that reaches more than 60% of the population. Next, we consider two scenarios with severe but shorter policy interventions, followed by a linear phased reduction (Figs. 4c and 4d); in the first scenario, the policy is less severe ($u(t) = 0.7$ vs. $u(t) = 1.2$ for 21 days), but the reduction period is longer (42 vs. 7 days) [64]. Comparing the two scenarios, we conclude that, provided that the initial policy interventions are sufficiently severe to ensure collective adoption of self-protections (thus avoiding the scenario shown in Fig. 4b), the successful eradication of the disease depends primarily on a sufficiently long phased reduction period. This avoids the multiple waves and subsequent lockdowns that would increase both the death toll and the total social-economic cost. The latter point is consistent with recent observations on the duration of policy interventions and their gradual uplifting during the COVID-19 pandemic [65]; however, there are far more epidemic complexities and real-world challenges to consider for COVID-19. Consistent with the SIS results, the SIR outcomes underline the key role of social influence, which may act as a double-edged sword, providing either a driving force or a retarding force for the collective adoption of self-protections, depending on whether the intervention policies are sufficiently strong.

These simulations illustrate the predictive power of our paradigm, once a proper parametrization and model have been extrapolated from empirical data. In fact, existing approaches typically estimate how infection parameters, associated with the disease dynamics, are explicitly changed due to policy interventions [19]. Generally, this is a difficult task that does not explicitly account for the complexity of human behavior. In contrast, our paradigm leaves the disease dynamics untouched, and allows policy interventions to only influence the decision-making process that determines the behavioral responses, which, in turn, shape the epidemic evolution.
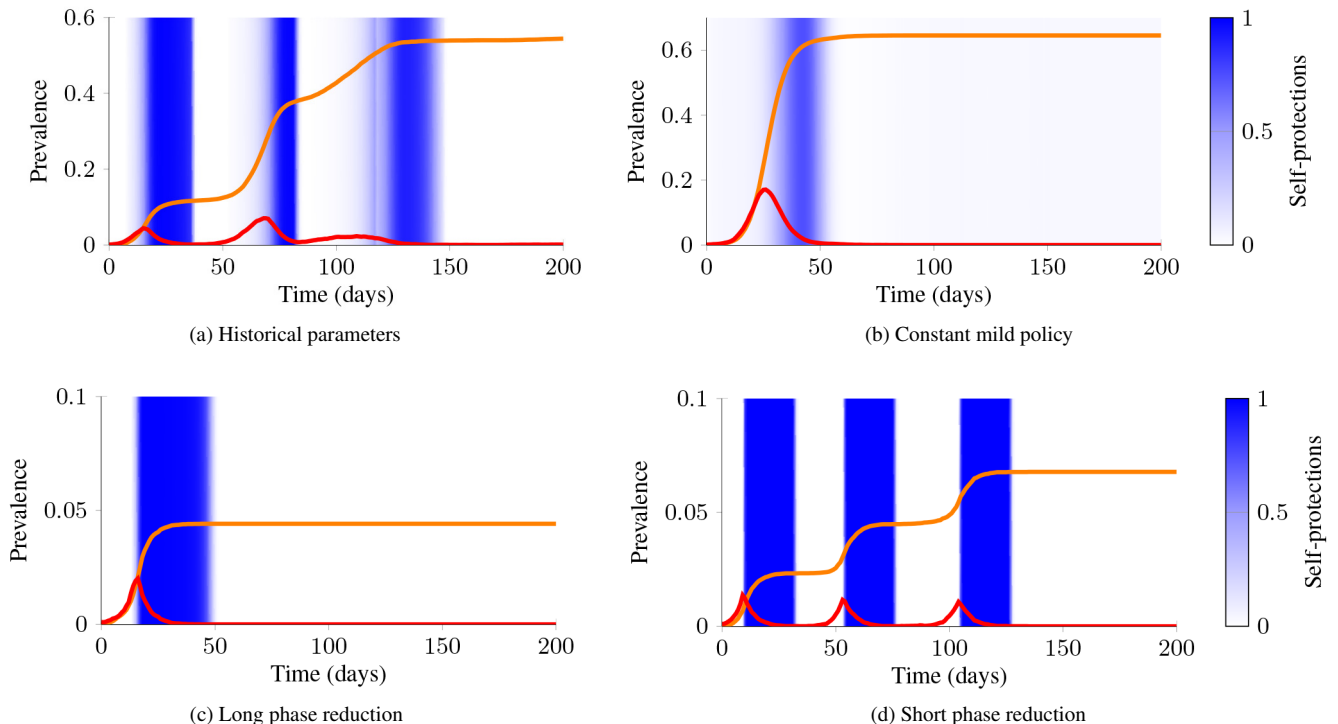
FIG. 4: Simulations of the SIR model. Temporal evolution of the epidemic prevalence $z(t)$ (red), recovered $R(t) := \frac{1}{n}|\{i : y_i(t) = R\}|$ (orange), and fraction of adopters of self-protections $\langle x(t) \rangle$ (intensity of the blue vertical bars) with (a) historical parameters of the 1918–19 Spanish flu pandemic [59, 60]; (b) a mild and constant intervention; (c) a severe intervention with a long phased reduction period; and (d) a very severe intervention with a short phased reduction period.

CONCLUSION

In summary, we proposed a novel and unified individual-level modeling paradigm that captures the co-evolution of disease spreading and collective decision-making at the same time scale. Our framework encapsulates a wide range of time-varying factors that are crucial in decision-making during epidemics, from the initial outbreak to its complete eradication, including government interventions, risk perception, bounded rationality, and social influence. The framework decouples the roles of these factors —which collectively shape the behavioral response to an epidemic outbreak— in an intuitive way, enabling their estimation from epidemiological [66], socio-demographic [61], communication [67], and mobility data [68], coupled with empirical studies on social influence [13], population adherence to NPIs [69, 70], risk perception [71], socio-economic impact of NPIs and emergence of distress [15, 48].

Our methodology is specifically designed to be a parsimonious paradigm, adaptable to different epidemic progression models [3, 33] and temporal network interactions [35, 37, 38, 40, 51]. Its simple formulation allows to perform fast simulations, scalable to large-scale systems. Complex real-world phenomena are reproduced within our unified framework — including periodic oscillations, multiple epidemic waves, and prompt collective response by the population leading to the fast eradication of the disease triggered by endogenous risk

perception or exogenous policy interventions. In particular, the paradigm allows to investigate the impact of different policy interventions on the collective behaviors and, in turn, on mitigating the spread.

Due to its flexibility, further features of the behavioral response can be directly incorporated in the paradigm, including mutual protection, delays in the behavioral response, and biased risk perceptions due to imperfect information on the epidemic prevalence. Finally, the combination of the proposed paradigm with more complex and realistic epidemic progression models (e.g., those tailored to COVID-19 [72, 73]) is key to further investigating the features captured by our model. This may allow our paradigm to be utilized to predict the behavioral response to real-world epidemic outbreaks and, thus, help public health authorities design effective interventions.

CONTRIBUTION STATEMENT

M.Y. and L.Z. contributed equally as leading authors. A.R. and M.C. contributed equally.

Appendix A: Derivation of Eq. (7)

In the absence of cumulative frustration and for a fully mixed influence layer, we observe that Eq. (1) has the same expression for all the individuals. In fact, if we define $\bar{x}(z)$ as the probability that a generic node adopts self-protective behaviors when the epidemic prevalence is equal to z, then, according to the strong law of large numbers, $\pi_i^0(t) = 1 - \bar{x}(z) - u(t) = 1 - \bar{x}(z) - \bar{u}$ (since the control is assumed to be constant) and $\pi_i^1(t) = \bar{x}(z) + r(z) - c$, which are independent of i. In a mean-field approach [54], we define $\theta(t) = \frac{1}{n}\sum_{i:y_i(t)=I} a_i$ as the average activity of infected nodes and $z_i(t) = \mathbb{P}[y_i(t) = I]$. Due to the strong law of large numbers, in the limit of large-scale systems $n \to \infty$, $z(t) = \frac{1}{n}\sum_{i=1}^n z_i(t)$ and $\theta(t) = \frac{1}{n}\sum_{i=1}^n a_i z_i(t)$. Hence, from the mean-field evolution of $z_i(t)$, given by

$$z_i(t+1) = z_i(t) - \mu z_i(t) + m\lambda(1 - z_i(t))(1 - \bar{x}(z(t)))\cdot \\ \cdot a_i z_i(t) + (1 - z_i(t))(1 - \bar{x}(z(t)))\lambda m\theta(t), \tag{A1}$$

we determine the following system of difference equations for the epidemic prevalence and the average activity of infected individuals, linearized about the disease-free equilibrium ($z = 0, \theta = 0$):

$$z(t+1) = z(t) - \mu z(t) + m\lambda\langle a\rangle z(t)(1 - \sigma\bar{x}(0)) \\ + m\lambda(1 - \sigma\bar{x}(0))\theta(t) \\ \theta(t+1) = \theta(t) - \mu\theta(t) + m\lambda\langle a^2\rangle z(t)(1 - \sigma\bar{x}(0)) \\ + m\lambda\langle a\rangle(1 - \sigma\bar{x}(0))\theta(t), \tag{A2}$$

where $\langle a\rangle$ and $\langle a^2\rangle$ are the average and second moment of the activity distribution, respectively.

From standard theory on the stability of discrete-time linear time-invariant systems [74], the origin is stable if

$$\frac{\lambda}{\mu} < \frac{1}{m(\langle a\rangle + \sqrt{\langle a^2\rangle})(1 - \sigma\bar{x}(0))}. \tag{A3}$$

In fully-mixed influence layers, the probability for an individual to adopt self-protective behaviors $\bar{x}(z)$ can be derived by substituting $\pi_i(0) = 1 - \bar{x}(z) - \bar{u}$ and $\pi_i(1) = \bar{x}(z) + r(z) - c$ into Eq. (1), obtaining the equilibrium equation:

$$\bar{x} = \frac{e^{\beta(\bar{x}-c+r(z))}}{e^{\beta(\bar{x}-c+r(z))} + e^{\beta(1-\bar{x}-\bar{u})}}. \tag{A4}$$

Even though it is not possible to derive a closed-form solution, we observe that at the inception of the epidemic outbreak, $x_i(0) = 0$ for all individuals and, for sufficiently small values of $\bar{u}$ (i.e., $\bar{u} \ll 1 + c$), in the early stages it is verified that $\pi_i^0(t) > \pi_i^1(t)$. Hence, if the rationality β is sufficiently large, the equilibrium $\bar{x}$ is close to 0 and can be approximated

by Taylor-expanding the right-hand side of the equation, obtaining

$$\bar{x}(z) \approx \frac{e^{\beta(-c+r(z))}}{e^{\beta(1-\bar{u})} + (1-\beta)e^{\beta(-c+r(z))}}, \tag{A5}$$

which can be evaluated for $z = 0$ and inserted into Eq. (A3), obtaining Eq. (7).

Appendix B: Parameters used in the simulations

Epidemic parameters

The SIS is calibrated on gonorrhea, which is a sexually transmitted disease characterized by negligible protective immunity after recovery and negligible latency period (individuals are infectious on average the day after contagion) [58, 75]. The SIR model is parametrized based on Spanish flu pandemic, which is characterized by a short latency period (individuals are infectious on average after 1–2 days from the contagion) that can be neglected and by protective immunity gained after recovery [59].

The epidemic parameters are set from epidemiological data. Specifically, reliable estimations of the time from infection to recovery τ are available [58, 59] (namely, $\tau = 55$ days for gonorrhea and $\tau = 4.1$ days for Spanish flu). Similar to Prem et al. [76], from these data we define $\mu = 1 - \exp(-1/\tau)$.

The parameter λ is obtained from available estimations of the basic reproduction number R_0 for the two diseases [58, 59] (namely, $R_0 = 1.6$ for gonorrhea and $R_0 = 2$ for Spanish flu). The basic reproduction number is defined as the average number of secondary infections produced by an infected individual in a population where everyone is susceptible. Hence, given that τ is the average time that an individual is infectious, assuming independence between the time an individual is infectious and their activity, we compute

$$R_0 = \frac{1}{n}\sum_{i\in\mathcal{V}}(a_i + \langle a\rangle)m\lambda\tau = 2\langle a\rangle m\lambda\tau, \tag{B1}$$

which implies $\lambda = R_0/2m\langle a\rangle\tau$. For the effectiveness of self-protective behaviors, we have assumed that they prevent 99% of the contagions in the SIS (gonorrhea) scenario, where self-protective behavior may include the use of physical protection barriers such as condoms). For the SIR model (Spanish flu), we assume a 95% effectiveness at preventing contagion, with self-protective behavior including physical distancing, stay-at-home actions, and wearing masks.

The epidemic parameters computed using this procedure are gathered in Table II.

Decision-making parameters

We set a common level of rationality $\beta = 6$ in all simulations, which captures a moderate level of rationality so that individuals tend to maximize their payoff, but always have a

TABLE II: Parameters used in the simulations.

Parameter	SIS (gonorrhea) [58]	SIR (Spanish flu) [59]
λ	0.3626	0.066
μ	0.1195	0.2164
σ	0.99	0.95
time unit	week	day

small but nonnegligible probability of adopting the behavior with the lower payoff. Before detailing the parameters used in the three case studies, we provide a brief discussion on the relative order of magnitude between the model parameters, which guided our choices.

The decision-making process is based on the comparison between the two payoff functions in Eqs. (2a)–(2b). The contribution of social influence to the payoff is always bounded between 0 and 1. Hence, social influence is significant if the other terms do not have a higher order of magnitude. Consequently, policy interventions $u(t) > 1$ can be considered severe, since their effect is predominant with respect to social influence, while policies with $u(t) < 1$ are milder. The cost of self-protective behaviors consists of two terms: the immediate cost per unit-time c and the accumulation factor γ. Small values of c become negligible in the decision making process, while, to avoid the immediate cost dominating the other terms, we should assume $c < 1$. The accumulation factor γ captures the cost for continued periods in which an individual adopts self-protective behaviors. To model a nonnegligible effect of the accumulation of socio-economic costs, we should guarantee that over long periods in which an individual consistently adopts self-protective behaviors, the frustration function saturates to a value comparable to the other terms. This can be achieved by imposing that

$$\lim_{t \to \infty} c + \sum_{s=1}^{t} \gamma^s c = \frac{c}{1 - \gamma} \approx 1 \,, \qquad \text{(B2)}$$

yielding $c + \gamma \approx 1$ (note, the above equality was obtained using the geometric series). Specifically, values of $\gamma > 1 - c$ guarantees that self-protective behaviors are eventually dismissed, after the complete eradication of the disease or the policy intervention is switched off. We use the risk perception function $r(t) = kz^{\alpha}$ with $\alpha = 1/2$ for cautious populations, $\alpha = 1$ to model proportional reactions, and $\alpha = 2$ for slow reacting populations. As discussed in the main article, the risk perception function determines a critical epidemic prevalence $z^* = \min\{z : r(z) > 1 + c\}$ that triggers the adoption of self-protective behaviors even in the absence of interventions (in the presence of accumulation, the immediate cost c in the expression of z^* is substituted by its saturation value from Eq. (B2), being $c/(1 - \gamma)$). We observe that risk perception becomes nonnegligible if $k > 1 + \frac{c}{1-\gamma}$. To keep consistency throughout our simulations, we set $k = 3$, which is

a value that verifies the condition above for all the choices of parameters c and γ we make in the simulations.

The decision-making parameters used for the two models are detailed in the following.

SIS model. We assume that the accumulation is negligible for gonorrhea (where the use of protections has an immediate cost that typically does not accumulate, such as protective sexual barriers). Hence, for all three simulations, we fix the immediate cost to $c = 0.3$ and the accumulation factor $\gamma = 0$. No policy intervention is set, with $u(t) = 0$ for all $t \geq 0$. In the three simulations, we test three different risk perception functions. Specifically, we consider a cautious population with $r(z) = 3\sqrt{z}$ in Figs. 3a and 3e, a population with a proportional reaction, $r(z) = 3z$ in Figs. 3b, 3d, 3f, and 3h, and a population slow to react with $r(z) = 3z^2$ in Figs. 3c and 3g.

SIR model. Self-protective behaviors involve social distancing and closures of economic activities, which has been shown to typically yield an accumulation of psychological distress and economic losses [15, 48, 63]. Hence, we assume a high accumulation factor $\gamma = 0.9$ and we fix $c = 0.12$, in light of our discussion above. To capture the slow reaction of the population due to the initial suppression of information (to keep morale up during World War I) [60, 77], we set $r(z) = 3z^2$. To further mirror real-world interventions by public authorities, in Fig. 4a, we set an initial intervention level equal to $u(0) = 0$, which switches to $u(t) = \bar{u} = 0.5$ once 1% of the population is infected and then remains active for 28 days before being turned off again, consistent with [60]. Then, we consider three different scenarios of intervention policies. In Fig. 4b, we set a constant mild level of interventions $u(t) = 0.4$, for all $t \geq 0$. In the other two scenarios, we set $u(0) = 0$. Then, in Fig. 4c, severe policies ($u(t) = 0.7$) are implemented for 21 days after reaching 1% of infections, after which $u(t)$ is linearly reduced to $u(t) = 0$ over 42 time-steps. In the second scenario (Fig. 4d), more severe policies ($u(t) = 1.2$) are implemented for the same period of 21 time-steps, after which $u(t)$ is linearly reduced to $u(t) = 0$ over a shorter time-window of 8 time-steps. Note that we select the intensity of policy interventions and the duration of the phased reduction to ensure that the cumulative intervention effort, $\sum_t u(t)$, over the duration of a lockdown, is equal to 29.4 in both scenarios.

Appendix C: Simulations without social influence

In the absence of social influence, the payoff functions reduces to

$$\pi_i^0(t) = -u(t), \qquad \pi_i^1(t) = r\big(z(t)\big) - f_i(t). \qquad \text{(C1)}$$

The simulations in Figs. 3d and 3h in the main article and in Fig. 5 are obtained utilizing the payoff functions in Eq. (C1).

[1] J. J. Van Bavel *et al.*, Nat. Hum. Behav. **4**, 460 (2020).

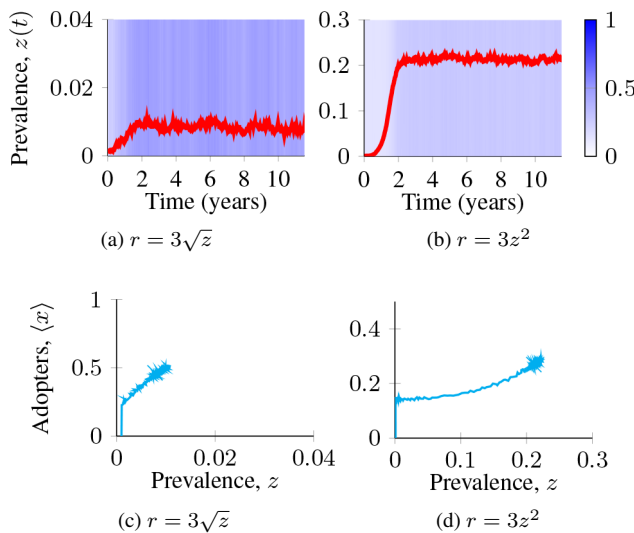[2] J. Bedson, L. A. Skrip, D. Pedi, S. Abramowitz, S. Carter, M. F.

FIG. 5: Simulations of the SIS model in the absence of social influence. In (a) and (b), we show the time-evolution of the epidemic prevalence $z(t)$ (red) and the fraction of adopters of self-protections $\langle x(t) \rangle$ (intensity of the blue bands). In (c) and (d), we show the corresponding trajectories on the phase-space. Panels refer to different risk perceptions $r(z)$, as detailed in the sub-captions.

Jalloh, S. Funk, N. Gobat, T. Giles-Vernick, G. Chowell, *et al.*, Nat. Hum. Behav. (2021).

[3] R. Pastor-Satorras, C. Castellano, P. Van Mieghem, and A. Vespignani, Rev. Mod. Phys. **87**, 925 (2015).

[4] S. Funk, M. Salathé, and V. A. Jansen, J. R. Soc. Interface **7**, 1247 (2010).

[5] N. Perra, D. Balcan, B. Gonçalves, and A. Vespignani, PLOS One **6** (2011).

[6] F. D. Sahneh, F. N. Chowdhury, and C. M. Scoglio, Sci. Rep. **2**, 632 (2012).

[7] C. Granell, S. Gómez, and A. Arenas, Phys. Rev. Lett. **111**, 128701 (2013).

[8] A. Rizzo, M. Frasca, and M. Porfiri, Phys. Rev. E **90**, 042801 (2014).

[9] Z. Wang, M. A. Andrews, Z.-X. Wu, L. Wang, and C. T. Bauch, Phys. Life Rev. **15**, 1 (2015).

[10] F. Verelst, L. Willem, and P. Beutels, J. R. Soc. Interface **13**, 20160820 (2016).

[11] J. S. Weitz, S. W. Park, C. Eksin, and J. Dushoff, Proc. Natl. Acad. Sci. USA **117**, 32764 (2020).

[12] N. Gozzi, M. Scudeler, D. Paolotti, A. Baronchelli, and N. Perra, Phys. Rev. E **104**, 014307 (2021).

[13] B. Tunçgenç, M. El Zein, J. Sulik, M. Newson, Y. Zhao, G. Dezecache, and O. Deroy, Br. J. Psychol. **112**, 763 (2021).

[14] P. Poletti, B. Caprile, M. Ajelli, A. Pugliese, and S. Merler, J. Theor. Biol. **260**, 31 (2009).

[15] M. Nicola, Z. Alsafi, C. Sohrabi, A. Kerwan, A. Al-Jabir, C. Iosifidis, M. Agha, and R. Agha, Int. J. Surg. **78**, 185 (2020).

[16] S. A. Pedro, F. T. Ndjomatchoua, P. Jentsch, J. M. Tchuenche, M. Anand, and C. T. Bauch, Front. Phys. **8**, 428 (2020).

[17] H. A. Simon, Mind Soc. **1**, 25 (2000).

[18] S. Flaxman, S. Mishra, A. Gandy, H. J. T. Unwin, T. A. Mellan, H. Coupland, C. Whittaker, H. Zhu, T. Berah, J. W. Eaton, *et al.*, Nature **584**, 257 (2020).

[19] N. Perra, Phys. Rep. **913**, 1 (2021).

[20] J. Piret and G. Boivin, Front. Microbiol. **11**, 3594 (2021).

[21] H. P. Young and S. Zamir, eds., *Handbook of Game Theory with Economic Applications*, Vol. 4 (Elsevier, 2015).

[22] K. M. A. Kabir and J. Tanimoto, R. Soc. Open Sci. **7**, 201095 (2020).

[23] J. Wei, L. Wang, and X. Yang, PLOS ONE **15**, 1 (2020).

[24] W. Just, J. Saldaña, and Y. Xin, J. Math. Biol. **76**, 1027 (2017).

[25] B. Steinegger, A. Arenas, J. Gómez-Gardeñes, and C. Granell, Phys. Rev. Research **2**, 023181 (2020).

[26] C. T. Bauch and D. J. D. Earn, Proc. Natl. Acad. Sci. USA **101**, 13391 (2004).

[27] F. Fu, D. I. Rosenbloom, L. Wang, and M. A. Nowak, Proc. Royal Soc. B **278**, 42 (2011).

[28] H.-F. Zhang, Z.-X. Wu, M. Tang, and Y.-C. Lai, Sci. Rep. **4**, 5666 (2014).

[29] H.-F. Zhang, P.-P. Shu, Z. Wang, M. Tang, and M. Small, Applied Mathematics and Computation **294**, 332 (2017).

[30] X. Chen and F. Fu, Proc. Royal Soc. B **286**, 20182406 (2019).

[31] S. L. Chang, M. Piraveenan, P. Pattison, and M. Prokopenko, J. Biol. Dyn. **14**, 57 (2020).

[32] C. R. Wells, A. Huppert, M. C. Fitzpatrick, A. Pandey, B. Velan, B. H. Singer, C. T. Bauch, and A. P. Galvani, Proc. Natl. Acad. Sci. USA **117**, 13138 (2020).

[33] F. Brauer and C. Castillo-Chavez, *Mathematical models in population biology and epidemiology* (Springer, 2012).

[34] S. Boccaletti, G. Bianconi, R. Criado, C. del Genio, J. Gómez-Gardeñes, M. Romance, I. Sendiña-Nadal, Z. Wang, and M. Zanin, Phys. Rep. **544**, 1 (2014).

[35] P. Holme and J. Saramäki, Phys. Rep. **519**, 97 (2012).

[36] N. Perra, B. Gonçalves, R. Pastor-Satorras, and A. Vespignani, Sci. Rep. **2**, 469 (2012).

[37] P. Holme, Eur. Phys. J. B **88**, 234 (2015).

[38] E. Valdano, L. Ferreri, C. Poletto, and V. Colizza, Phys. Rev. X **5**, 021005 (2015).

[39] L. Zino, A. Rizzo, and M. Porfiri, Phys. Rev. Lett. **117**, 228302 (2016).

[40] A. Koher, H. H. K. Lentz, J. P. Gleeson, and P. Hövel, Phys. Rev. X **9**, 031017 (2019).

[41] L. Blume, Games Econ. Behav. **11**, 111 (1995).

[42] M. O. Jackson and Y. Zenou, in *Handbook of Game Theory with Economic Applications*, Vol. 4 (Elsevier, 2015) Chap. 3, pp. 95–163.

[43] R. B. Cialdini and N. J. Goldstein, Annu. Rev. Psychol. **55**, 591 (2004).

[44] H. Peyton Young, Annu. Rev. Econ. **7**, 359 (2015).

[45] H. P. Young, Econometrica , 57 (1993).

[46] A. Montanari and A. Saberi, Proc. Natl. Acad. Sci. USA **107**, 20196 (2010).

[47] H. Peyton Young, Am. Econ. Rev. **99**, 1899 (2009).

[48] J. Qiu, B. Shen, M. Zhao, Z. Wang, B. Xie, and Y. Xu, Gen. Psychiatr. **33**, e100213 (2020).

[49] A. Rizzo, B. Pedalino, and M. Porfiri, J. Theor. Biol. **394**, 212 (2016).

[50] I. Pozzana, K. Sun, and N. Perra, Phys. Rev. E **96**, 042310 (2017).

[51] L. Zino, A. Rizzo, and M. Porfiri, SIAM J. Appl. Dyn. Syst. **17**, 2830 (2018).

[52] G. Petri and A. Barrat, Phys. Rev. Lett. **121**, 228301 (2018).

[53] J. Leitch, K. A. Alexander, and S. Sengupta, Appl. Netw. Sci. **4**, 105 (2019).

[54] P. Van Mieghem, J. Omic, and R. Kooij, IEEE/ACM Trans. Netw. **17**, 1 (2009).

[55] The code is available at https://github.com/lzino90/behavior.

[56] D. J. Watts and S. H. Strogatz, Nature **393**, 440 (1998).

[57] W. Aiello, F. Chung, and L. Lu, Exp. Math. **10**, 53 (2001).

[58] J. A. Yorke, H. W. Hethcote, and A. Nold, Sex. Transm. Dis. **5**, 51 (1978).

[59] C. E. Mills, J. M. Robins, and M. Lipsitch, Nature **432**, 904 (2004).

[60] H. Markel, H. B. Lipman, J. A. Navarro, A. Sloan, J. R. Michalsen, A. M. Stern, and M. S. Cetron, JAMA **298**, 644 (2007).

[61] J. Mossong, N. Hens, M. Jit, P. Beutels, K. Auranen, R. Mikolajczyk, M. Massari, S. Salmaso, G. S. Tomba, J. Wallinga, *et al.*, PLOS Med. **5**, e74 (2008).

[62] J. M. Barry, Nature **459**, 324 (2009).

[63] A. W. Bartik, M. Bertrand, Z. Cullen, E. L. Glaeser, M. Luca, and C. Stanton, Proc. Natl. Acad. Sci. USA **117**, 17656 (2020).

[64] The total control efforts for the two policies, measured as the sum of $u(t)$ over the duration of a lockdown, are the same.

[65] L. López and X. Rodó, Nat. Hum. Behav. **4**, 746 (2020).

[66] S. Cobey, Science **368**, 713 (2020).

[67] N. Oliver, B. Lepri, H. Sterly, R. Lambiotte, S. Deletaille, M. De Nadai, E. Letouzé, A. A. Salah, R. Benjamins, C. Cattuto, *et al.*, Sci. Adv. **6**, eabc0764 (2020).

[68] Google, "COVID-19 Community Mobility Reports," `https://www.google.com/covid19/mobility` (2021).

[69] N. Haug, L. Geyrhofer, A. Londei, E. Dervic, A. Desvars-Larrive, V. Loreto, B. Pinior, S. Thurner, and P. Klimek, Nat. Hum. Behav. **4**, 1303 (2020).

[70] S. Singh, M. Shaikh, K. Hauck, and M. Miraldo, Proc. Natl. Acad. Sci. USA **118** (2021).

[71] S. Dryhurst, C. R. Schneider, J. Kerr, A. L. J. Freeman, G. Recchia, A. M. van der Bles, D. Spiegelhalter, and S. van der Linden, J. Risk Res. **23**, 994 (2020).

[72] E. Estrada, Phys. Rep. **869**, 1 (2020).

[73] A. Arenas, W. Cota, J. Gómez-Gardeñes, S. Gómez, C. Granell, J. T. Matamalas, D. Soriano-Paños, and B. Steinegger, Phys. Rev. X **10**, 041055 (2020).

[74] W. Rugh, *Linear System Theory*, Vol. 2 (Prentice Hall, Upper Saddle River, NJ, 1996).

[75] A. Lajmanovich and J. A. Yorke, Math. Biosci. **28**, 221 (1976).

[76] K. Prem, Y. Liu, T. W. Russell, A. J. Kucharski, R. M. Eggo, N. Davies, S. Flasche, S. Clifford, C. A. B. Pearson, J. D. Munday, *et al.*, Lancet Public Health **5**, e261 (2020).

[77] M. C. J. Bootsma and N. M. Ferguson, Proc. Natl. Acad. Sci. USA **104**, 7588 (2007).